Temporal instability of viscous liquid microjets with spatially varying surface tension

2005 J. Phys. A: Math. Gen. 38 263

(http://iopscience.iop.org/0305-4470/38/1/020)

INSTITUTE OF PHYSICS PUBLISHING JOURNAL OF PHYSICS A: MATHEMATICAL AND GENERAL

J. Phys. A: Math. Gen. **38** (2005) 263–276 doi:10.1088/0305-4470/38/1/020

Temporal instability of viscous liquid microjets with spatially varying surface tension

E P Furlani

Integrated Materials and Microstructures Laboratory, Electronic Imaging Products, Eastman Kodak Company, Rochester, NY 14650-2121, USA

E-mail: edward.furlani@kodak.com

Received 14 March 2004, in final form 1 November 2004
Published 8 December 2004
Online at stacks.iop.org/JPhysA/38/263

Abstract

A linear theory is developed for the temporal instability of a viscous liquid microjet of Newtonian fluid with a spatially periodic variation of surface tension imposed along its length. The variation of surface tension induces Marangoni flow within the jet that leads to breakup and drop formation. An analytical expression is derived for the behaviour of the free surface of the microjet. This expression is useful for parametric analysis of jet instability and breakup as a function of jet radius, wavelength and fluid properties.

PACS numbers: 47.10.+g, 47.20.Dr, 47.20.Gv, 68.03.Cd

Introduction

Liquid jets are inherently unstable and can be induced to breakup by various means such as a perturbation of the free surface, the application of pressure or velocity variations along the jet, or fluctuations in fluid properties. The analysis of jet instability dates back to Lord Rayleigh, and an historical overview of the progress in this field has been summarized by Ashgriz and Mashayek [1, 2]. While some of the effects that cause jet instability have been studied extensively, others have not [3]. In particular, relatively few authors have studied jet instability due to spatial variations of surface tension, despite the practical relevance of this phenomenon. Specifically, advances in microsystems technology have enabled the development of microfluidic inkjet printing elements with thousands of functional microjets that can be individually controlled to produce steady steams of picoliter sized droplets at kilohertz frequency rates by applying a periodic thermal modulation to the surface of each microjet as it exits an orifice [4–7]. The thermal energy imparted to the jet is carried downstream by its velocity. Since the surface tension of the jet is temperature dependent, the advection of thermal energy gives rise to a time-dependent spatially periodic variation (or gradient) of surface tension along the free surface. This gradient in surface tension

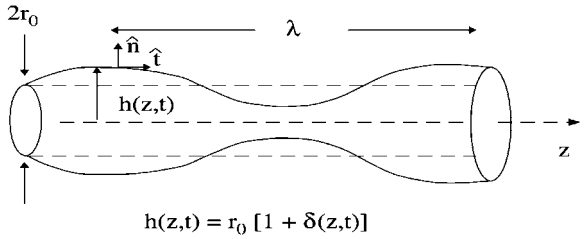

Figure 1. Jet geometry.

gives rise to a shear stress at the free surface, which is balanced by inertial forces in the fluid, thereby inducing a Marangoni flow towards regions of higher surface tension. This, in turn, produces a deformation of the free surface that ultimately leads to instability and drop formation. A rigorous analysis of this phenomenon requires the solution of a fully coupled thermal/fluid/free-surface boundary value problem that takes into account flow through the orifice, thermal diffusion within the orifice manifold and reservoir, thermal diffusion and advection in the microjet, and complex free-surface dynamics. While this phenomenon holds substantial potential for unprecedented versatility and speed in inkjet applications and merits this level of rigor, such analysis is beyond the scope of this paper.

In this paper we study the temporal instability of an infinite viscous microjet that is subjected to a spatially periodic variation of surface tension along its length. We start with the linearized axisymmetric Navier–Stokes equations for a Newtonian fluid, and derive analytical expressions for the time dependence of the jet velocity and free surface. While other authors have studied this phenomenon, the analytical expression presented here is new [8]. Moreover, it provides insight into underlying physical effects and is useful for rapid parametric analysis of jet instability as a function of the jet radius, modulation wavelength and fluid properties. We demonstrate the theory with some sample calculations, and show that as a microjet approaches breakup it swells at points of maximum surface tension and necks at points of minimum surface tension. Lastly, we modify the theory to account for a thermally induced modulation of surface tension, and use this to estimate the time to drop formation and drop volume for inkjet applications.

Theory

In this section we solve the equation of motion governing the behaviour of the free surface of an infinite axisymmetric viscous microjet of Newtonian fluid with a spatially periodic variation of surface tension imposed along its length (figure 1).

We neglect the effects of gravity, and obtain the following system of equations for a jet of incompressible fluid with surface tension σ, viscosity μ and density ρ:

Navier–Stokes

$$\rho\frac{\mathrm{D}v}{\mathrm{D}t} = -\nabla p + \mu\nabla^2 v, \tag{1}$$

where

$$\frac{\mathrm{D}}{\mathrm{D}t} = \frac{\partial}{\partial t} + v\cdot\nabla.$$

Continuity

$$\nabla \cdot v = 0. \tag{2}$$

Boundary conditions

The boundary conditions for this problem include stress balance, a kinematic condition and axisymmetric flow conditions. The first two conditions apply at the free surface (liquid–gas interface), while the flow conditions apply along the axis of the microjet. The first boundary condition, stress balance, can be written as [9]

$$\hat{n} \cdot \mathbf{T} = -2H\sigma\hat{n} + \nabla_s\sigma, \tag{3}$$

where $\mathbf{T}$ is the stress tensor in the fluid (we assume that the external gas is stress free), $\sigma(z)$ is the surface tension,

$$H = \frac{1}{2}\left(\frac{1}{h(1+h'^2)^{1/2}} + \frac{h''}{(1+h'^2)^{3/2}}\right), \tag{4}$$

and $\hat{n}$ and $\hat{t}$ are unit vectors normal and tangential to the free surface (figure 1),

$$\hat{n} = \hat{r}\frac{1}{\sqrt{1+h'^2}} - \hat{z}\frac{h'}{\sqrt{1+h'^2}}, \tag{5}$$

$$\hat{t} = \hat{r}\frac{h'}{\sqrt{1+h'^2}} + \hat{z}\frac{1}{\sqrt{1+h'^2}}. \tag{6}$$

The surface gradient ∇_s is

$$\nabla_s = \hat{r}\frac{h'}{(1+h'^2)}\frac{\partial}{\partial z} + \hat{\theta}\frac{1}{h}\frac{\partial}{\partial\theta} + \hat{z}\frac{1}{(1+h'^2)}\frac{\partial}{\partial z}. \tag{7}$$

In these expressions $h(z,t)$ defines the radial position of the free surface, and $h' = \frac{\partial h}{\partial z}$. Equation (3) can be decomposed into normal and tangential components:

$$(\hat{n} \cdot \mathbf{T}) \cdot \hat{n} = -2H\sigma, \qquad \text{(normal stress)} \tag{8}$$

$$(\mathbf{T} \cdot \hat{n}) \cdot \hat{t} = \hat{t} \cdot \nabla_s\sigma, \qquad \text{(tangential stress)} \tag{9}$$

where

$$\hat{t} \cdot \nabla_s\sigma = \frac{1}{\sqrt{1+h'^2}}\frac{\partial\sigma}{\partial z}. \tag{10}$$

The gradient of surface tension $\nabla_s\sigma$ produces a Marangoni flow towards regions of higher surface tension which deform the free surface of the jet and ultimately causes breakup. The second (kinematic) boundary condition implies that fluid does not cross the free surface,

$$\frac{\mathrm{D}}{\mathrm{D}t}(r - h(z,t)) = 0 \qquad (r = h). \tag{11}$$

The flow conditions along the axis of the jet are

$$v_r = 0, \qquad (r = 0) \tag{12}$$

and

$$\frac{\partial v_z}{\partial r} = 0 \qquad (r = 0). \tag{13}$$

Solution method

Our solution method follows a radial expansion approach described by Eggers [10, 11]. First, we write all equations in component form. For axisymmetric flow, the Navier–Stokes equation (1) reduces to

$$\rho\left(\frac{\partial v_r}{\partial t}+v_r\frac{\partial v_r}{\partial r}+v_z\frac{\partial v_r}{\partial z}\right)=-\frac{\partial p}{\partial r}+\mu\left[\frac{\partial}{\partial r}\left(\frac{1}{r}\frac{\partial(rv_r)}{\partial r}\right)+\frac{\partial^2 v_r}{\partial z^2}\right], \tag{14}$$

and

$$\rho\left(\frac{\partial v_z}{\partial t}+v_r\frac{\partial v_z}{\partial r}+v_z\frac{\partial v_z}{\partial z}\right)=-\frac{\partial p}{\partial z}+\mu\left[\frac{1}{r}\frac{\partial}{\partial r}\left(r\frac{\partial v_z}{\partial r}\right)+\frac{\partial^2 v_z}{\partial z^2}\right]. \tag{15}$$

The continuity condition (2) becomes

$$\frac{1}{r}\frac{\partial(rv_r)}{\partial r}+\frac{\partial v_z}{\partial z}=0. \tag{16}$$

The normal and tangential stress boundary conditions (8) and (9) can be written as

$$p+\frac{2\mu}{(1+h'^2)}\left[h'\left(\frac{\partial v_z}{\partial r}+\frac{\partial v_r}{\partial z}\right)-\frac{\partial v_r}{\partial r}-h'^2\frac{\partial v_z}{\partial z}\right]$$
$$=-\sigma\left[\frac{1}{h(1+h'^2)^{1/2}}-\frac{h''}{(1+h'^2)^{3/2}}\right]\quad(r=h), \tag{17}$$

and

$$\frac{\mu}{(1+h'^2)}\left[2h'\left(\frac{\partial v_r}{\partial r}-\frac{\partial v_z}{\partial z}\right)+(1-h'^2)\left(\frac{\partial v_r}{\partial z}+\frac{\partial v_z}{\partial r}\right)\right]=\frac{1}{\sqrt{1+h'^2}}\frac{\partial\sigma}{\partial z}(r=h). \tag{18}$$

Similarly, the kinematic condition (11) gives

$$\frac{\partial h}{\partial t}+v_z h'=v_r\qquad(r=h). \tag{19}$$

We seek a solution to equations (14)–(19). To this end, we expand $v_z(r,z,t)$ and $p(r,z,t)$in powers of r

$$v_z(r,z,t)=v_0(z,t)+v_2(z,t)r^2+\cdots, \tag{20}$$
$$p(r,z,t)=p_0(z,t)+p_2(z,t)r^2+\cdots. \tag{21}$$

From the continuity condition (2) and the expansion (20) we obtain

$$v_r(r,z,t)=-\frac{\partial v_0(z,t)}{\partial z}\frac{r}{2}-\frac{\partial v_2(z,t)}{\partial z}\frac{r^3}{4}+\cdots. \tag{22}$$

Note that these expansions are compatible with the boundary conditions (12) and (13).
Using expansions (20)–(22) we find that the equation of motion (14) for v_r is identically satisfied to lowest order. However, equation (15) for v_z gives

$$\frac{\partial v_0}{\partial t}+v_0\frac{\partial v_0}{\partial z}=-\frac{1}{\rho}\frac{\partial p_0}{\partial z}+\frac{\mu}{\rho}\left(4v_2+\frac{\partial^2 v_0}{\partial z^2}\right). \tag{23}$$

To solve for v_0 we need to eliminate the second-order term v_2 from (23). To this end, we evaluate the tangential stress condition (18) at $r=h$, collect lowest order terms and obtain

$$v_2=\frac{1}{2\mu h}\frac{\partial\sigma}{\partial z}+\frac{3}{2h}\frac{\partial h}{\partial z}\frac{\partial v_0}{\partial z}+\frac{1}{4}\frac{\partial^2 v_0}{\partial z^2}. \tag{24}$$

Furthermore, from the normal stress boundary condition (17) we find that

$$p_0 = -\mu \frac{\partial v_0}{\partial z} + 2\sigma H. \tag{25}$$

We substitute (24) and (25) into (23) and obtain

$$\frac{\partial v_0}{\partial t} + v_0 \frac{\partial v_0}{\partial z} = -\frac{1}{\rho}\frac{\partial}{\partial z}(2\sigma H) + \frac{2}{\rho h}\frac{\partial \sigma}{\partial z} + \frac{3\mu}{\rho h^2}\frac{\partial}{\partial z}\left(h^2 \frac{\partial v_0}{\partial z}\right). \tag{26}$$

Finally, the kinematic condition (19) gives

$$\frac{\partial h}{\partial t} = -v_0 \frac{\partial h}{\partial z} - \frac{h}{2}\frac{\partial v_0}{\partial z}. \tag{27}$$

Equations (26) and (27) can be reduced further using the following expansions,

$$v_0(z,t) = v_0 + u(z,t), \tag{28}$$

$$h(z,t) = r_0[1 + \delta(z,t)], \tag{29}$$

and

$$\sigma(z) = \sigma_0 + \sigma_1(z), \tag{30}$$

where r_0, v_0 and σ_0 are the unperturbed radius, velocity and surface tension of the jet, respectively, and $u(z,t)$, $\delta(z,t)$ and $\sigma_1(z)$ are perturbations to these values. To simplify the analysis we transform to a coordinate system at rest with respect to the jet,

$$\eta = z - v_0 t. \tag{31}$$

We use (28), (29), (30) and (31) in (26) and (27), and then linearize the resulting equations by ignoring products of derivatives, etc. The linearized equations (26) and (27) reduce to

$$\frac{\partial u}{\partial t} - \frac{\sigma_0}{\rho r_0}\left[\frac{\partial \delta}{\partial \eta} + r_0^2 \frac{\partial^3 \delta}{\partial \eta^3}\right] - \frac{3\mu}{\rho}\frac{\partial^2 u}{\partial \eta^2} = \frac{1}{\rho r_0}\frac{\partial \sigma_1}{\partial \eta}, \tag{32}$$

and

$$\frac{\partial^2 u}{\partial \eta^2} = -2\frac{\partial^2 \delta}{\partial \eta \partial t}. \tag{33}$$

We combine (32) and (33) into a single equation by applying $\frac{\partial}{\partial \eta}$ to (32) and then substituting (33) into the resulting equation. This gives

$$\frac{\partial^2 \delta}{\partial t^2} + \frac{\sigma_0}{2\rho r_0}\left[\frac{\partial^2 \delta}{\partial \eta^2} + r_0^2 \frac{\partial^4 \delta}{\partial \eta^4}\right] - \frac{3\mu}{\rho}\frac{\partial^3 \delta}{\partial \eta^2 \partial t} = -\frac{1}{2\rho r_0}\frac{\partial^2 \sigma_1}{\partial \eta^2}. \tag{34}$$

This is the equation of motion for $\delta(\eta, t)$ which defines the free surface. For a well-posed problem we need to specify initial conditions for $\delta(\eta, t)$, and a functional dependence for $\sigma_1(\eta)$. We choose the following,

$$\delta(\eta, 0) = 0, \tag{35}$$

$$\frac{\partial}{\partial t}\delta(\eta, 0) = 0, \tag{36}$$

and

$$\sigma_1(\eta) = -\frac{\Delta\sigma}{2}\left(1 + \cos\left(\frac{2\pi}{\lambda}\eta\right)\right). \tag{37}$$

Equations (34), (35) and (36) define an initial-value problem for $\delta(\eta, t)$. It is important to note that conditions (35) and (36) imply that there is no initial perturbation to the free

surface. The jet instability studied here is initiated by a variation in surface tension that induces Marangoni flow within the jet towards regions of higher surface tension, which, in turn, causes a deformation of the free surface that leads to breakup.

The solution to (34) can be decomposed into a homogeneous and particular part. The homogeneous solution satisfies

$$\frac{\partial^2\delta}{\partial t^2} + \frac{\sigma_0}{2\rho r_0}\left[\frac{\partial^2\delta}{\partial\eta^2} + r_0^2\frac{\partial^4\delta}{\partial\eta^4}\right] - \frac{3\mu}{\rho}\frac{\partial^3\delta}{\partial\eta^2\partial t} = 0. \tag{38}$$

Based on the form of $\sigma_1(\eta)$ we seek a solution of the form

$$\delta_h(\eta, t) = \mathrm{e}^{\alpha t}\cos\left(\frac{2\pi}{\lambda}\eta\right). \tag{39}$$

We substitute (39) into (38) and find that

$$\alpha^2 + \frac{3\mu}{\rho}\left(\frac{2\pi}{\lambda}\right)^2\alpha - \beta^2 = 0, \tag{40}$$

where

$$\beta^2 = \frac{\sigma_0}{2\rho r_0}\left(\frac{2\pi}{\lambda}\right)^2\left\{1 - r_0^2\left(\frac{2\pi}{\lambda}\right)^2\right\}. \tag{41}$$

There are two solutions to (40),

$$\alpha_\pm = \frac{-\frac{3\mu}{\rho}\left(\frac{2\pi}{\lambda}\right)^2 \pm \sqrt{\left[\frac{3\mu}{\rho}\left(\frac{2\pi}{\lambda}\right)^2\right]^2 + 4\beta^2}}{2}. \tag{42}$$

Thus, the homogeneous solution is of the form

$$\delta_h(\eta, t) = [A\,\mathrm{e}^{\alpha_+ t} + B\,\mathrm{e}^{\alpha_- t}]\cos\left(\frac{2\pi}{\lambda}\eta\right), \tag{43}$$

where A and B are arbitrary constants. It is easy to show that the particular solution is of the form

$$\delta_p(\eta) = \frac{\sigma}{4\rho r_0\beta^2}\left(\frac{2\pi}{\lambda}\right)^2\cos\left(\frac{2\pi}{\lambda}\eta\right). \tag{44}$$

Thus, the general solution is

$$\delta(\eta, t) = [A\,\mathrm{e}^{\alpha_+ t} + B\,\mathrm{e}^{\alpha_- t}]\cos\left(\frac{2\pi}{\lambda}\eta\right) + \frac{\Delta\sigma}{4\rho r_0\beta^2}\left(\frac{2\pi}{\lambda}\right)^2\cos\left(\frac{2\pi}{\lambda}\eta\right). \tag{45}$$

The constants A and B are determined from the initial conditions (35) and (36). After some algebra we find that

$$\delta(\eta, t) = \frac{\Delta\sigma}{2\sigma_0}\frac{1}{\left[1 - r_0^2\left(\frac{2\pi}{\lambda}\right)^2\right]}\left[1 + \frac{\alpha_-}{\alpha_+ - \alpha_-}\mathrm{e}^{\alpha_+ t} - \frac{\alpha_+}{\alpha_+ - \alpha_-}\mathrm{e}^{\alpha_- t}\right]\cos\left(\frac{2\pi\eta}{\lambda}\right). \tag{46}$$

This expression describes the behaviour of the free surface $h(\eta, t) = r_0[1 + \delta(\eta, t)]$. For a given time $t > 0$ the function $\delta(z, t)$ obtains a maximum when $\eta \equiv \eta_{\max} = \pm\frac{\lambda}{2}, \pm\frac{3\lambda}{2}, \pm\frac{5\lambda}{2}, \ldots$, and a minimum when $\eta \equiv \eta_{\min} = 0, \pm\lambda, \pm 2\lambda, \pm 3\lambda, \ldots$. Jet breakup (pinch-off) occurs when $\delta(\eta_{\max}, t) = 1$ or $\delta(\eta_{\min}, t) = -1$ (i.e., when $h(\eta, t) = 2r_0$ or 0, respectively). Thus, for example, the time to breakup T_b can be computed by solving for the value of $t = T_\mathrm{b}$ that gives $\delta(\eta = 0, t) = -1$. Equation (46) is a key result. It enables rapid parametric analysis of jet instability and breakup as a function of r_0, λ, and fluid properties. We demonstrate its use in the next section.

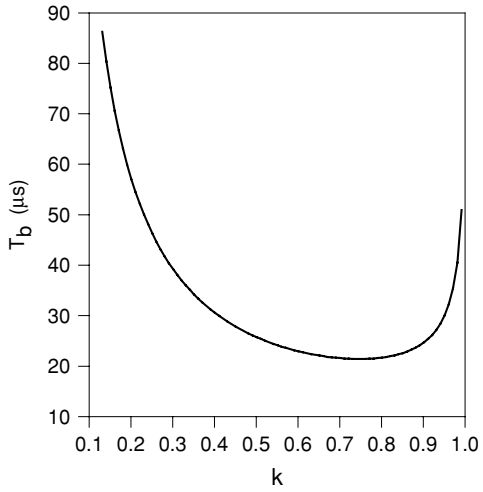

Figure 2. Time to breakup versus wavenumber.

It is also instructive to solve for the velocity $u(\eta, t)$. We substitute (46) into (33) and obtain

$$u(\eta, t) = -\frac{\Delta\sigma}{\sigma_0}\frac{\lambda}{2\pi}\frac{\alpha_+\alpha_-}{(\alpha_+ - \alpha_-)}\frac{1}{\left[1 - r_0^2\left(\frac{2\pi}{\lambda}\right)^2\right]}[e^{\alpha_+ t} - e^{\alpha_- t}]\sin\left(\frac{2\pi\eta}{\lambda}\right). \quad (47)$$

This expression gives the variation in jet velocity $u(\eta, t)$ as measured by an observer moving with velocity v_0.

Results

The analytical solution (46) enables rapid parametric analysis of jet breakup. We demonstrate it via application to a microjet of water with $\mu = 0.001\ \mathrm{N\,s\,m^{-2}}$, $\rho = 1000\ \mathrm{kg\,m^{-3}}$, $r_0 = 5\ \mu\mathrm{m}$, $v_0 = 10\ \mathrm{m\,s^{-1}}$, $\sigma_0 = 0.073\ \mathrm{N\,m^{-1}}$. We compute the time to breakup T_b by setting $\eta = 0$ in (46) and solving for the value $t = T_\mathrm{b}$ that gives $\delta(\eta = 0, t) = -1$. First, we compute T_b as a function of the reduced wavenumber $k = 2\pi r_0/\lambda$ for $0 \leqslant k \leqslant 1$, i.e., for a range of wavelengths $\lambda \geqslant 2\pi r_0$ (figure 2).

From this analysis we find that the jet is most sensitive to breakup at a wavenumber $k = 0.731$ ($\lambda = 8.6\, r_0$). This is also evident from a plot of the dimensionless growth rate parameter $\alpha_+\sqrt{\rho\, r_0^3/\sigma_0}$ (figure 3).

Next, we fix $\lambda = 8.6\, r_0$ and compute T_b as a function of the percent variation in surface tension with $0.001 < \Delta\sigma/\sigma_0 < 0.5$. Note that T_b increases nonlinearly with decreasing σ (figure 4).

It is also instructive to plot T_b as a function of normalized viscosity μ/μ_0 and density ρ/ρ_0 where $\mu_0 = 0.001\ \mathrm{N\,s\,m^{-2}}$ and $\rho_0 = 1000\ \mathrm{kg\,m^{-3}}$ (figures 5 and 6). These plots show that T_b increases with viscosity and density as expected due to the associated increase in viscous damping and inertia, respectively. A similar trend is observed in a plot of T_b versus jet radius, which also reflects an increase in inertia with r_0 (figure 7).

Next, we plot the normalized jet profile, $r/r_0 = (1 + \delta(\eta, t))$, as a function of $x = \eta/\lambda$ for $-1 < x < 1$ ($-\lambda < \eta < \lambda$), with $t = 0$, $0.75T_\mathrm{b}$, and T_b (figure 8). Note that the jet necks at points $\eta = 0, \pm\lambda, \pm 2\lambda, \pm 3\lambda, \ldots$, where σ is a minimum ($\sigma = \sigma_0 - \Delta\sigma$), and swells at

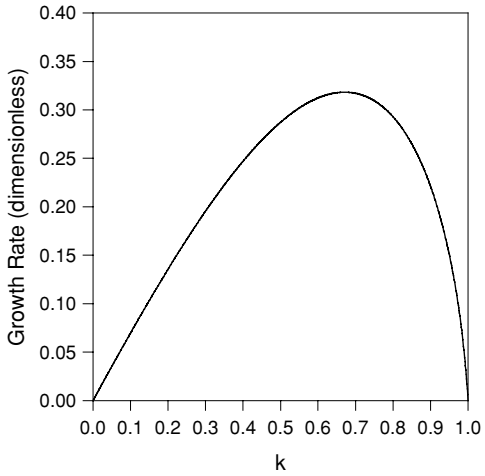

Figure 3. Dimensionless growth rate versus wavenumber.

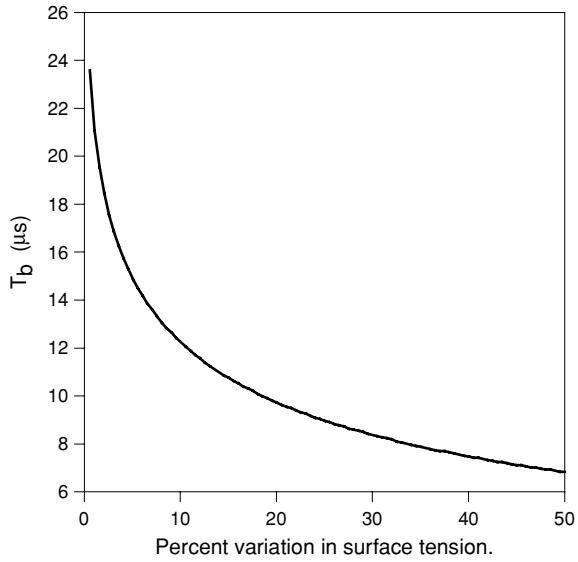

Figure 4. Time to breakup versus per cent variation in surface tension.

points $\eta = \pm\frac{\lambda}{2}, \pm\frac{3\lambda}{2}, \pm\frac{5\lambda}{2}, \ldots$, where σ is a maximum ($\sigma = \sigma_0$). Lastly, we track r/r_0 as a function time at the pinch-off point $\eta = 0$. The radial decay is initially gradual, but increases rapidly as t approaches T_b (figure 9).

Applications

In this section we modify the free-surface equation (46) for inkjet applications. There are two issues to address before we begin the analysis. First, this equation predicts the instability of an infinite jet in which the deformation of the free surface grows in a periodic fashion along the entire length of the jet, whereas in inkjet applications the jet emanates from a nozzle

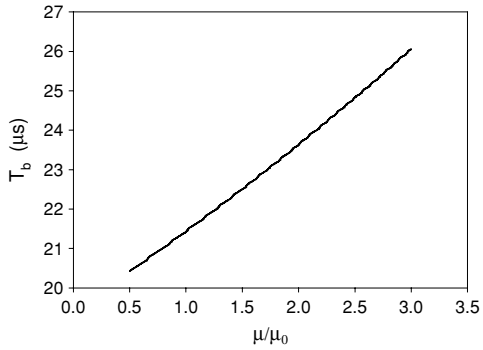

Figure 5. Time to breakup versus normalized viscosity.

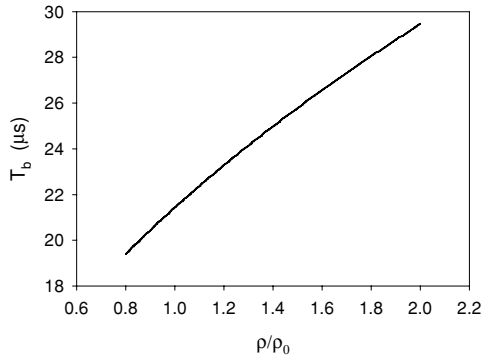

Figure 6. Time to breakup versus normalized density.

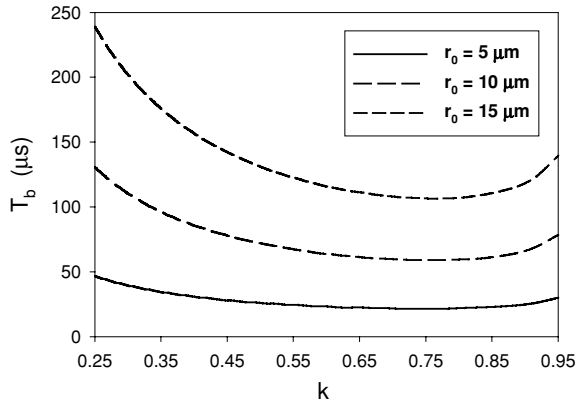

Figure 7. Time to breakup versus k and jet radius.

and the deformation of the free surface grows with increasing distance from the nozzle. The former is known as temporal instability, while the latter is known as spatial instability. Second, equation (46) is based on linear theory, but the jet breakup process is nonlinear. Regarding the first issue, it has been proven that spatial and temporal instability analysis predict the same time to breakup T_b as long as the jet velocity v_0 is much greater than the capillary velocity

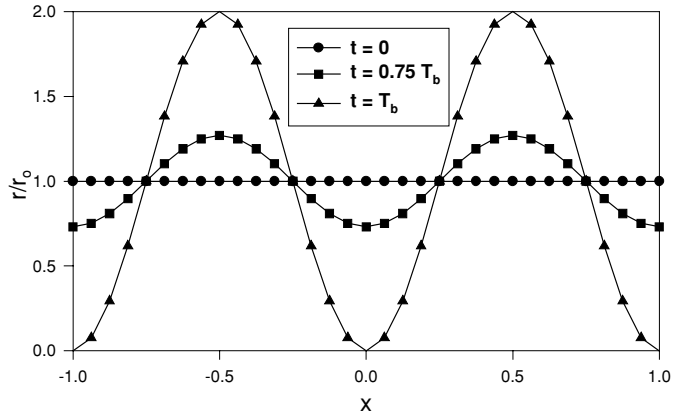

Figure 8. Normalized jet profile at different times.

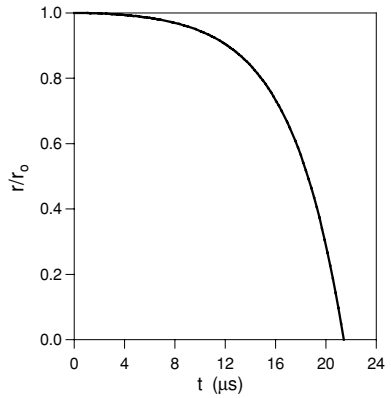

Figure 9. Normalized jet radius at neck point versus time.

$v_c = \sqrt{\sigma/(\rho r_0)}$ [12]. For inkjet applications v_0 is typically between 10 and 20 m s^{-1} while $v_c \approx 2$ m s^{-1}, and this condition is reasonably well satisfied. Regarding the second issue, linear analysis applies as long as the deformation of the free surface $\delta(\eta, t)$ is small relative to the unperturbed radius r_0. Now, in inkjet applications the applied perturbation is small $\Delta\sigma \ll \sigma_0$, and the jet remains substantially cylindrical up until breakup, at which point there is a dramatic short-lived pinch-off process. While linear analysis does not apply to the final stage of pinch-off, the duration of this process is small compared to the total breakup time, and therefore linear theory gives a very reasonable estimate of T_b, which has been verified experimentally [13].

We are now ready to modify equation (46) for inkjet applications. As noted above, microfluidic inkjet printing elements can produce streams of picoliter-sized droplets via thermal modulation of surface tension. These silicon-based inkjet elements consist of a reservoir connected to a planar orifice manifold with thousands of individual orifices, typically greater than 10 μm in diameter. The reservoir is pressured to produce an array of microjets with velocities in the range of 10–20 m s^{-1}. Each orifice has a heating element associated with it (either embedded within the manifold or deposited on its surface, near the orifice), and each heating element can be individually actuated to heat the surface of the microjet as it

exits the orifice. The thermal energy, which is applied in a timewise fashion at the orifice, is carried downstream by the fluid velocity, and dissipates from the surface by convection into the surrounding air (convection coefficient h_{conv}), and diffusion into the microjet (diffusivity α). Both of these processes are slow compared to the downstream advection. For example, the thermal energy deposited on the surface of a microjet of water ($\alpha = 1.47 \times 10^{-7}$ m^2 s^{-1}) with a diameter $2r_0 = 10$ μm and jet velocity $v_0 = 10$ m s^{-1} will travel a distance $z = 100$ μm downstream in 10 μs, but will only diffuse a distance of approximately $l_d(t) \approx \sqrt{\alpha\, t} = 1.2$ μm into the jet during this time. Thus, the microjet develops a time-dependent temperature profile $T(r, z, t)$ along its length that gradually decreases in magnitude, and is predominantly confined to an annulus $r_h(t) \leqslant r \leqslant r_0$ where $r_h(t) \approx r_0 - l_d(t)$.

The variation of surface temperature $T(r_0, z, t)$ induces a time-dependent variation of surface tension along the microjet, which, in turn, induces thermal Marangoni convection within the microjet. To first order,

$$\sigma(T) = \sigma_0 - C_\sigma(T - T_0), \tag{48}$$

where $\sigma(T)$ is the surface tension at temperature T, σ_0 is the surface tension at the ambient temperature T_0 and C_σ is a constant. Therefore, in a periodically heated inkjet, the surface tension $\sigma(T(r_0, z, t))$ depends on both position and time. This induces instability within the microjet resulting in a deformation of the free surface that grows with increasing distance from the orifice. However, equation (46) cannot be directly applied to inkjet applications because it is based on the assumption that the magnitude of the applied perturbation $\Delta\sigma$ is constant in time, whereas in inkjet applications $\Delta\sigma$ is time-dependent due to thermal diffusion. In the following, we adapt our theory to account for this time dependence.

To understand the time dependence of surface tension in ink jet applications, we need to consider the way in which heat is imparted to a microjet to cause drop formation. In practice, the heater is activated for a time τ_{on} and then deactivated for a time τ_{off} in a cyclic fashion. This produces a time-dependent spatially periodic temperature profile along the jet with a wavelength of approximately $\lambda = v_0\,\tau_h$ where $\tau_h = \tau_{\mathrm{on}} + \tau_{\mathrm{off}}$. At any instant of time, the induced temperature profile along the microjet can be considered to be of the form

$$T(r, z) = T_0 - T_\Delta(z)\, f(r) \tag{49}$$

where T_0 is the ambient temperature, and

$$T_\Delta(z) = \frac{\Delta T}{2}\left(1 + \cos\left(\frac{2\pi}{\lambda}z\right)\right), \tag{50}$$

with

$$f(r) = \begin{cases} 0 & (r < r_h) \\ 1 & (r \geqslant r_h). \end{cases} \tag{51}$$

We evaluate (49) at $r = r_0$ and substitute the result into (48) which gives

$$\begin{aligned} \sigma(z) &= \sigma_0 - \frac{C_\sigma \Delta T}{2}\left(1 + \cos\left(\frac{2\pi}{\lambda}z\right)\right), \\ &= \sigma_0 - \frac{\Delta\sigma}{2}\left(1 + \cos\left(\frac{2\pi}{\lambda}z\right)\right), \end{aligned} \tag{52}$$

where $\Delta\sigma = C_\sigma \Delta T$. Note that (52) is the same as (30) with $\sigma_1(z)$ given by (37). Thus, the thermally induced modulation of surface tension in inkjet applications is related to our linear theory. It remains to account for the time decay of $T_\Delta(r, z, t)$.

Consider the diffusion of thermal energy in an infinite insulated column of stationary fluid of radius r_0 with an initial temperature given by (49). The temperature distribution $T_\Delta(r, z, t)$

within the fluid satisfies the following boundary value problem,

$$\frac{\partial^2 T_\Delta}{\partial r^2}+\frac{1}{r}\frac{\partial T_\Delta}{\partial r}+\frac{\partial^2 T_\Delta}{\partial z^2}=\frac{1}{\alpha}\frac{\partial T_\Delta}{\partial t} \qquad 0\leqslant r\leqslant r_0, \quad -\infty<z<\infty, \quad t>0, \tag{53}$$

$$T_\Delta(r,z,0)=\begin{cases}0 & (0<r<r_h)\\ \dfrac{\Delta T}{2}\left(1+\cos\left(\dfrac{2\pi}{\lambda}z\right)\right) & (r_h\leqslant r\leqslant r_0)\end{cases} \tag{54}$$

$$\frac{\partial T_\Delta}{\partial r}=0 \qquad (r=r_0). \tag{55}$$

The solution to (53)–(55) is

$$T_\Delta(r,z,t)=\frac{\Delta T}{2}\left[\frac{r_0^2-r_h^2}{r_0^2}+\frac{2}{r_0^2}\sum_{m=1}^{\infty}c_m\,\mathrm{e}^{-\alpha\gamma_m^2 t}J_0(\gamma_m r)\right]\left(1+\mathrm{e}^{-\alpha(2\pi/\lambda)^2 t}\cos\left(\frac{2\pi}{\lambda}z\right)\right), \tag{56}$$

where $J_n(\gamma_m r)$ is the Bessel function of order n, γ_m are the positive roots of $J_1(\gamma_m r_0)=0$ and $c_m=\frac{1}{J_0^2(\gamma_m r_0)}\int_{r_h}^{r_0} r' J_0(\gamma_m r')\,\mathrm{d}r'$. We are interested in the surface temperature $T_\Delta(r_0,z,t)$. It is easy to verify that $\gamma_m^2\gg(2\pi/\lambda)^2$ for all m ($\lambda\geqslant 2\pi r_0$). Thus, we neglect terms containing $\mathrm{e}^{-\alpha(2\pi/\lambda)^2 t}$, and obtain an estimate for the time decay of the temperature variation at the surface,

$$\Delta T_s(t)\approx\frac{\Delta T}{2}\left[\frac{r_0^2-r_h^2}{r_0^2}+\frac{2}{r_0^2}\sum_{m=1}^{\infty}c_m\,\mathrm{e}^{-\alpha\gamma_m^2 t}J_0(\gamma_m r_0)\right]. \tag{57}$$

We use this in equation (52) to estimate the decay rate of $\Delta\sigma$,

$$\Delta\sigma(t)=\Delta\sigma\left[\frac{r_0^2-r_h^2}{r_0^2}+\frac{2}{r_0^2}\sum_{m=1}^{\infty}c_m\,\mathrm{e}^{-\alpha\gamma_m^2 t}J_0(\gamma_m r_0)\right]. \tag{58}$$

Finally, we substitute (58) into (46) and obtain an expression for the deformation of the free surface that accounts for thermal diffusion,

$$\delta_h(\eta,t)=\frac{\Delta\sigma}{2\sigma_0}\frac{\left[\frac{r_0^2-r_h^2}{r_0^2}+\frac{2}{r_0^2}\sum_{m=1}^{\infty}c_m\,\mathrm{e}^{-\alpha\gamma_m^2 t}J_0(\gamma_m r_0)\right]}{\left[1-r_0^2\left(\frac{2\pi}{\lambda}\right)^2\right]} \times\left[1+\frac{\alpha_-}{\alpha_+-\alpha_-}\mathrm{e}^{\alpha_+ t}-\frac{\alpha_+}{\alpha_+-\alpha_-}\mathrm{e}^{\alpha_- t}\right]\cos\left(\frac{2\pi\eta}{\lambda}\right). \tag{59}$$

In this expression $r_h\approx r_0-\sqrt{\alpha\tau_{\mathrm{on}}}$ where $\lambda=v_0\tau_h$, v_0 is the jet velocity, τ_{on} is the duration of the heat pulse, and τ_h is the period of the heating cycle. We use (59) to estimate the time to drop formation for inkjet applications. As an example, consider a microjet of water with $\mu=0.001\ \mathrm{N\,s\,m^{-2}}$, $\rho=1000\ \mathrm{kg\,m^{-3}}$, $r_0=5\ \mu\mathrm{m}$, $v_0=10\ \mathrm{m\,s^{-1}}$, $\sigma_0=0.073\ \mathrm{N\,m^{-1}}$, and $\Delta\sigma/\sigma_0=0.01$. We compute T_{b} as a function of wavenumber $k=2\pi r_0/\lambda$ with and without the thermal diffusion (figure 10). Note that the minima of these plots occur at the same wavelength $\lambda_{\min}\approx 8.6\,r_0$. However, the breakup with thermal diffusion is slower because of the decay of $\Delta\sigma$. To achieve $\lambda_{\min}$ we set $\tau_h=\lambda_{\min}/v_0=4.3\ \mu\mathrm{s}$ with $\tau_{\mathrm{on}}\approx\tau_h/2$. This gives a drop production frequency $f=1/\tau_h=232$ kHz, and a drop volume $V_{\mathrm{drop}}\approx\pi r_0^2\lambda\times 10^{-3}=3.3$ picoliters. It is useful to determine the scaling of key inkjet variables as a function of orifice radiusr_0. It is easy to verify that $\tau_h\propto r_0$, $f\propto 1/r_0$,$V_{\mathrm{drop}}\propto r_0^3$. Also T_{b} decreases with r_0 but in a more complex fashion. These relations show that higher operating frequencies, shorter breakup lengths and smaller drop sizes can be obtained with smaller orifices.

Finally, equation (59) enables rapid parametric analysis of drop production as a function of operating frequency, jet radius, temperature modulation and fluid properties. It should be of considerable use in the development of novel microfluidic inkjet systems.

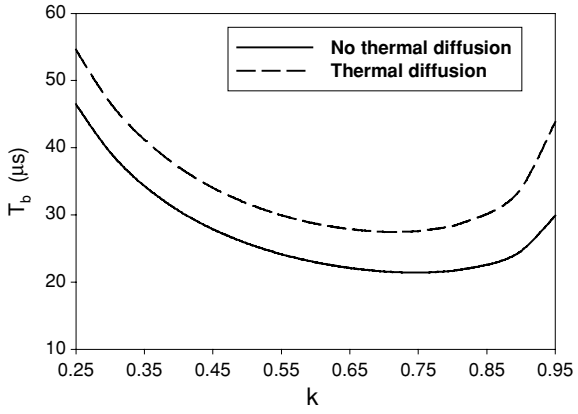

Figure 10. Time to breakup versus k with/without thermal diffusion.

Conclusions

We have studied the behaviour of a slender microjet of Newtonian fluid with a spatially periodic variation of surface tension imposed along its length. We have derived an analytical expression for the time dependence of the free surface, and used this to perform rapid parametric analysis of jet instability and pinch-off. We have shown that as the jet approaches breakup it swells at points of maximum surface tension, and necks at points of minimum surface tension. We have also adapted the theory for use in inkjet applications. In such applications the jet instability is initiated by Marangoni flow that is induced by a thermal modulation of surface tension. We consider the diffusion of thermal energy within the jet and obtain an expression for the time dependence of its surface temperature. This gives an estimate of the time dependence of the surface tension, which leads to an equation for the behavior of the thermally modulated free-surface. We use this to estimate the time to drop formation and drop volume for novel inkjet applications.

Acknowledgments

The author would like to thank Professors Osman Basaran and Michael Brenner, and Christopher Delametter, James Chwalek, and David Trauernicht, for numerous valuable technical discussions. The author would also like to thank Edward J Furlani for help with the preparation of this manuscript.

References

[1] Lord Rayleigh 1879 On the instability of jets *Proc. Lond. Math. Soc.* **10** 4–13
[2] Ashgriz N and Mashayek F 1995 Temporal analysis of capillary jet breakup *J. Fluid Mech.* **291** 163
Rayleigh Lord 1879 On the instability of jets *Proc. Lond. Math. Soc.* **10** 4–13
[3] Middleman S 1995 *Modeling Axisymmetric Flows; Dynamics of Films, Jets and Drops* (New York: Academic)
[4] Chwalek J M, Trauernicht D P, Delametter C N, Sharma R, Jeanmaire D L, Anagnostopoulos C N, Hawkins G A, Ambravaneswaran B, Panditaratne J C and Basaran O A 2002 A new method for deflecting liquid microjets *Phys. Fluids* **14** 37
[5] Trauernicht D P, Delametter C N, Chwalek J M, Jeanmaire D L and Anagnostopoulos C N 2001 *IS&T Non-Impact Printing 17 (Fort Lauderdale, FL)* (Springfield, VA: The Society for Imaging Science and Technology) p 295

[6] Chwalek J M, Trauernicht D P, Delametter C N, Jeanmaire D L and Anagnostopoulos C N 2001 *IS&T Non-Impact Printing 17 (Fort Lauderdale, FL)* (Springfield, VA: The Society for Imaging Science and Technology) p 291
[7] Furlani E P, Delametter C N, Chwalek J M and Trauernicht D P 2001 *Fourth Int. Conf. on Modeling and Simulation of Microsystems (Hilton Head, SC)* (Cambridge, MA: Appl. Comp. Res. Society) p 186
[8] Bauer H F 1984 Free liquid surface response induced by fluctuations of thermal marangoni convection *AIAA J.* **22** 421–8
[9] Dean W M 1998 *Analysis of Transport Phenomena* (New York: Oxford University Press)
[10] Eggers J 1993 Universal pinching of 3D axisymmetric free-surface flow *Phys. Rev. Lett.* **71** 3458
[11] Eggers J 1997 Nonlinear dynamics and breakup of free-surface flows *Rev. Mod. Phys.* **69** 865
[12] Keller J B, Rubinow S I and Tu Y O 1973 Spatial instability of a jet *Phys. Fluids* **16** 2052
[13] Kalaaji A, Lopez B, Attane P and Soucemarianadin A 2003 Breakup length of forced liquid jets *Phys. Fluids* **15** 2469